Supplementary Materials

A Highly Emissive Zn(II)-pyridyl-benzimidazolyl-phenolato based Chemosensor: Detection of $H_2PO_4^-$ via "Use" and "Throw" Device Fabrication

Sunanda Dey, Sukanya Paul, Kingshuk Debsharma, Chittaranjan Sinha*

Table S1 Crystal data and refine parameters for probe HL.

Empirical formula	$C_{27}H_{23}N_3O_2$
Formula weight	421.48
Temperature (K)	273(2)
System	orthorhombic
Space group	$P2_12_12_1$
a (Å)	9.0805(9)
b (Å)	10.1637(10)
c (Å)	23.374(2)
$\alpha=\beta=\gamma$ /°	90
V $(Å)^3$	2157.2 (4)
Z	4
D(cal)/g cm^{-3}	1.298
μ/mm^{-1}	0.083
λ(Å)	0.71073
data[$I > 2\sigma(I)$]/params	3805/279
Final R indices [I $>2\sigma(I)$][a,b]	R_1= 0.1007 wR_2= 0.1951
GOF[c]	1.118

[a]$R_1 = \Sigma||F_o|-|F_c||/\Sigma|F_o|$; [b]$wR_2 = \{\Sigma[w(F_o^2-F_c^2)^2]/\Sigma[w(F^2_o)^2]\}^{1/2}$; $w = [\sigma^2(F_o)^2 + (0.1003P)^2 + 4.9693P]^{-1}(F_o^2 + 2F_c^2)/3$; [c] Goodness-of-fit

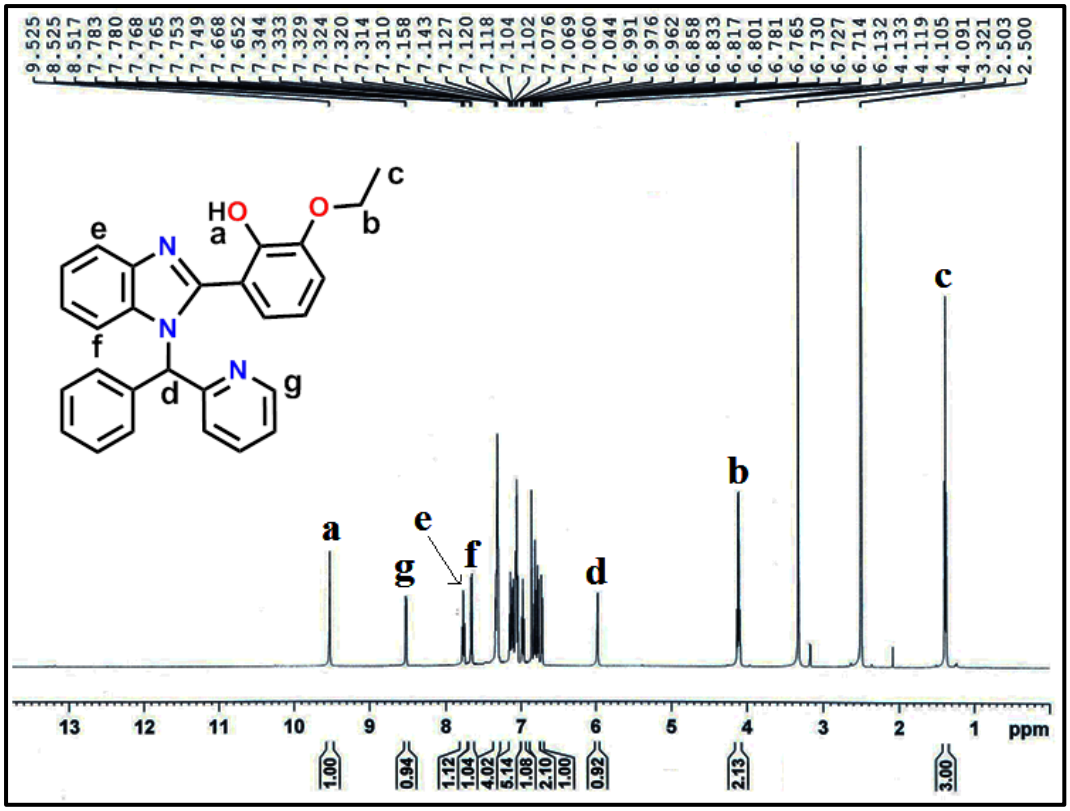

Fig. S1 ^{1}H NMR spectrum of HL.

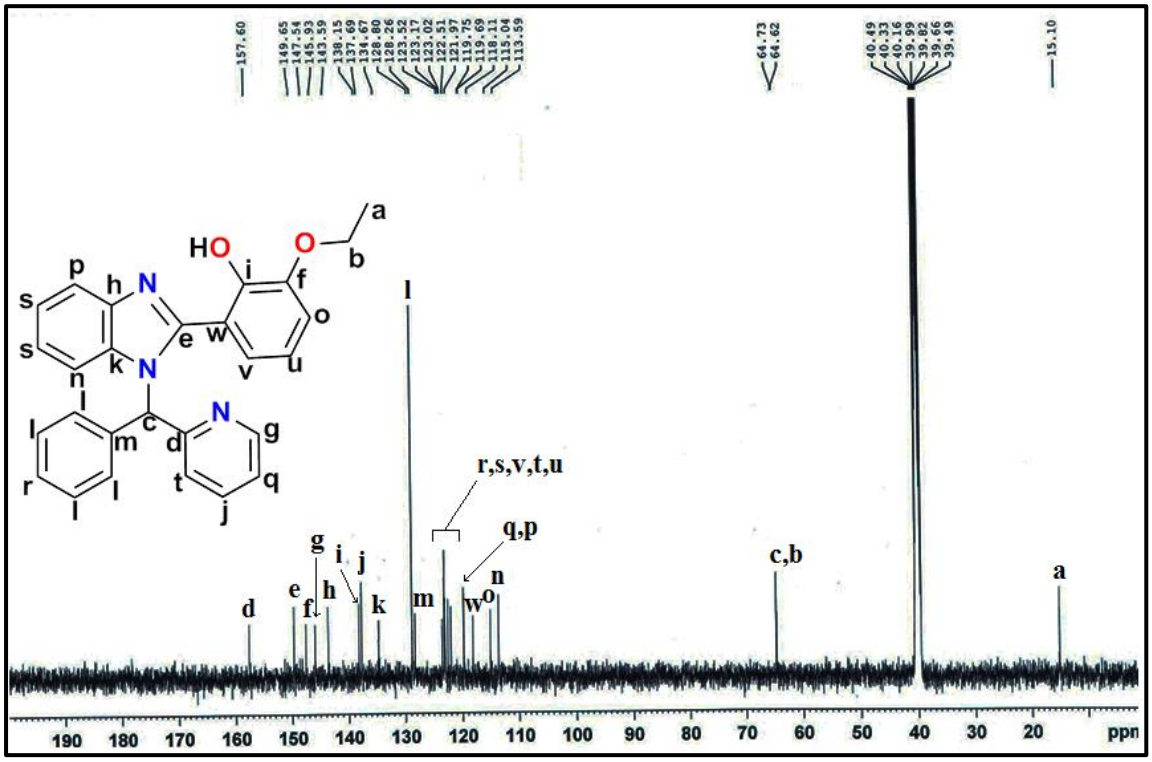

Fig. S2 ^{13}C NMR spectrum of HL.

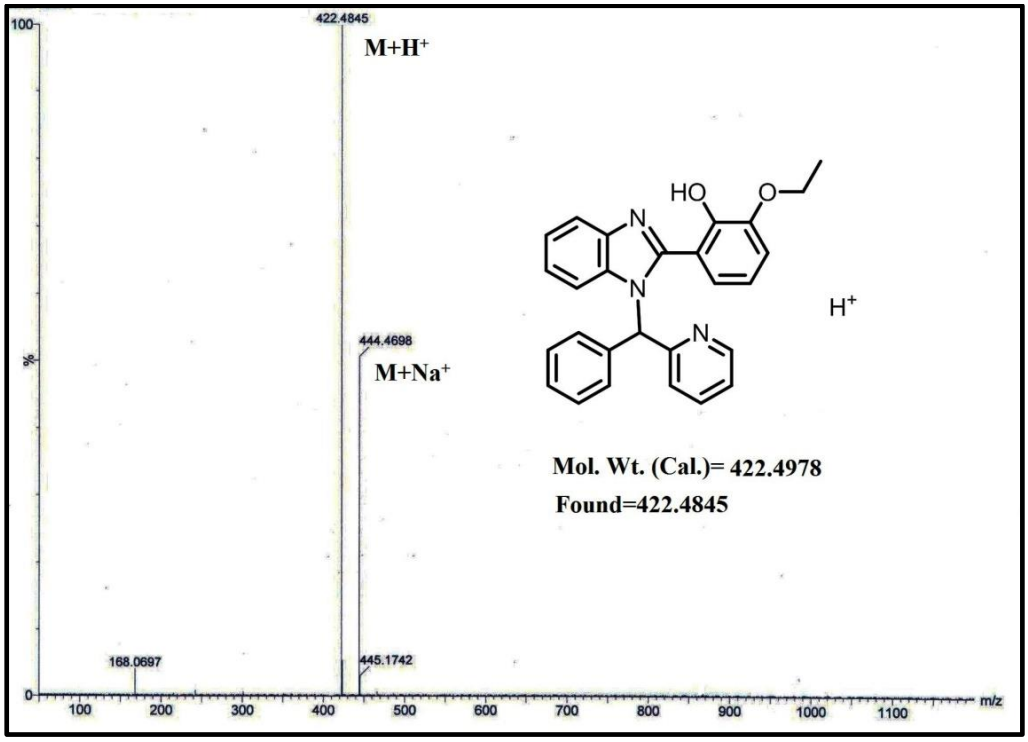

Fig. S3 ESI-MS spectrum of HL.

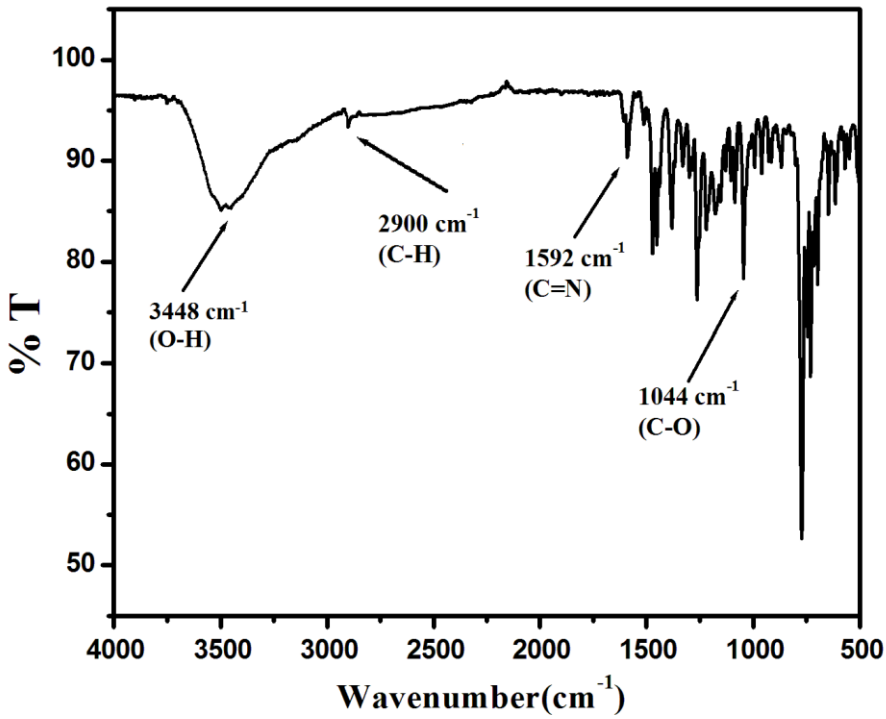

Fig. S4 IR Spectrum of HL.

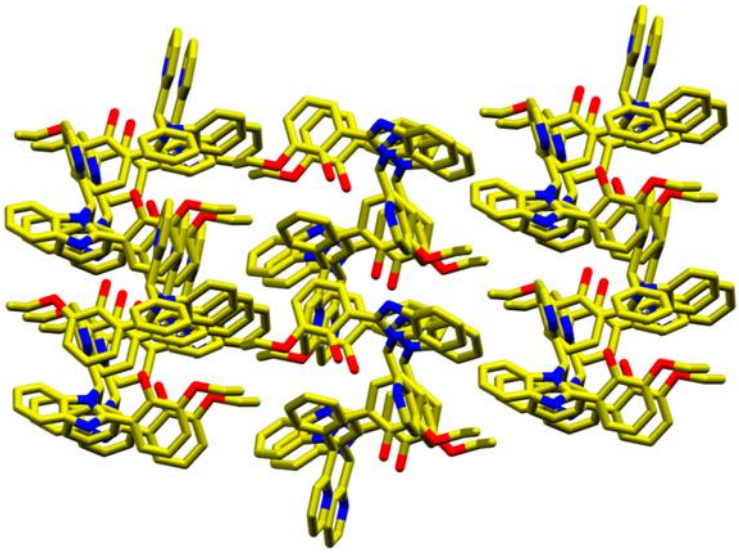

Fig S5 Supramolecular assembly of HL along 'c-axis'.

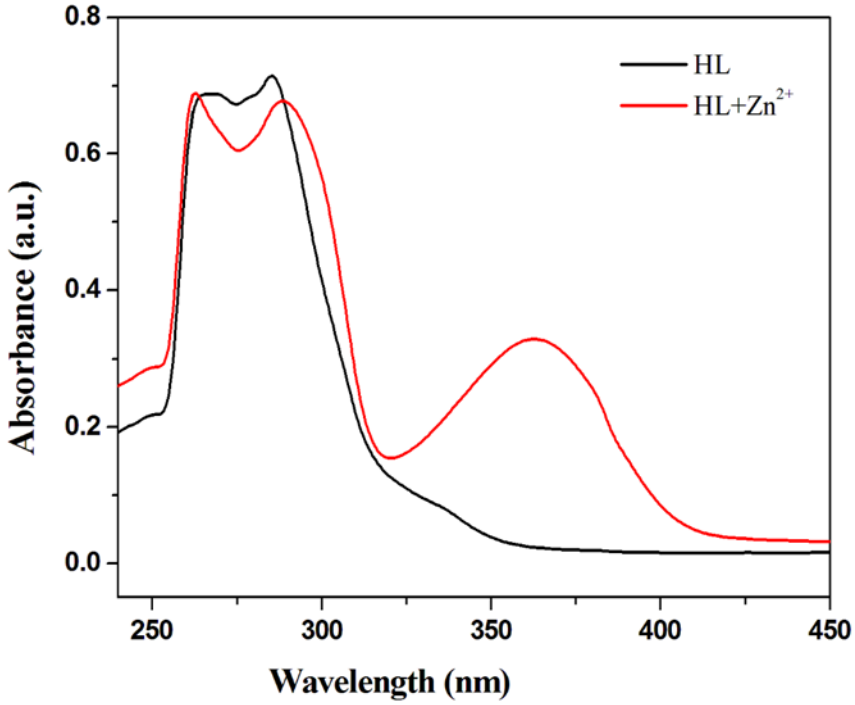

Fig. S6 Change in the absorption spectrum of HL (50 µM) on gradual addition of Zn^{2+} (0-50 µM); inset: absorption spectrum of HL and its Zn-complex.

Table S2 Some selective torsional angles present in the free probe HL (obtained from X-Ray structure).

Bonds	Angle (°)
C8 N1 C7 C18	47.3(10)
N2 C007 C5 C4	58.1(10)
N1 C7 C19 C24	57.1(7)
N2 C007 C5 C6	-116.5(8)
N1 C7 C18 N3	38.1(9)
N1 C7 C18 C17	-144.1(7)
N1 C7 C19 C20	-121.6(6)
N1 C007 C5 C4	-121.2(8)
C007 N1 C7 C19	86.5(8)
N1 C007 C5 C6	64.2(10)

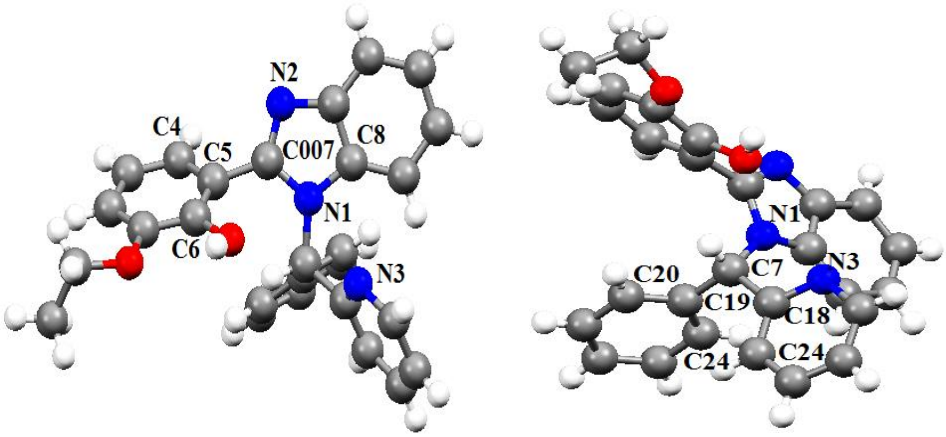

Fig. S7 X-Ray structure of HL exhibiting twisting framework (two different view).

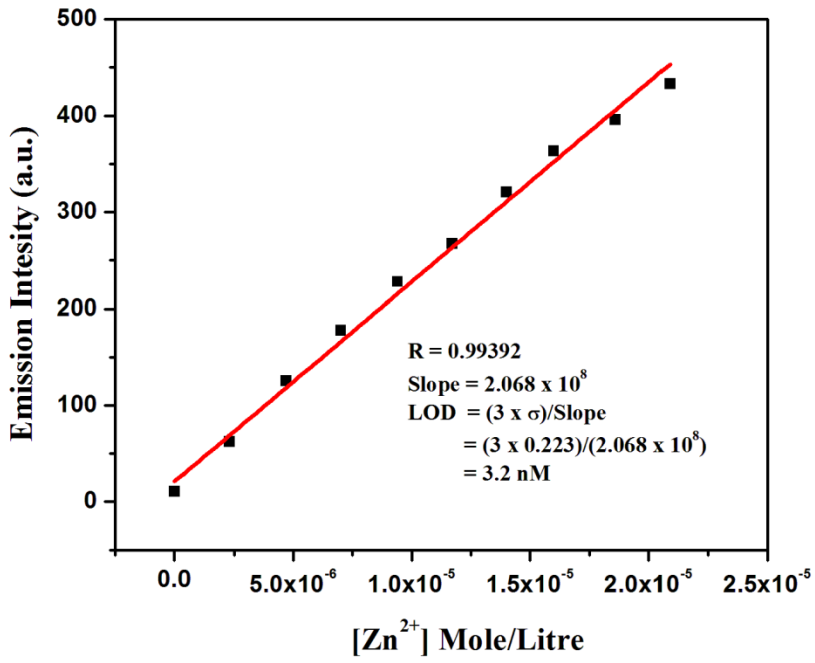

Fig. S8 Limit of detection (LOD) for Zn^{2+} by the probe, HL.

Table S3 Some of the reported $Zn^{2+}/H_2PO_4^-$ selective probe along with LOD.

SL No.	Probe	Selectivity (LOD)	Solvent	Ref.
1.	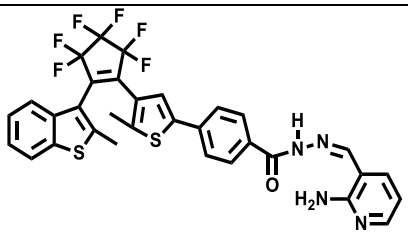	Zn^{2+} (0.562 μM) $H_2PO_4^-$ (0.0314 μM) HSO_4^- (0.0304 μM)	CH_3CN	[1]
2.	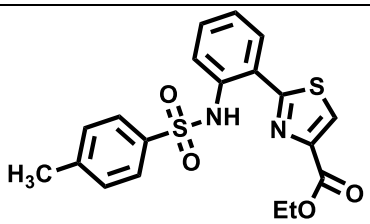	Zn^{2+} (20 μM) $HP_2O_7^{3-}$ (1 μM) $H_2PO_4^-$ (1 μM)	EtOH	[2]
3.	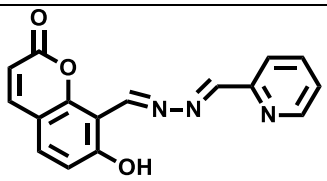	Zn^{2+} (0.103 μM) HPO_4^{2-} (0.207 μM)	DMF/HEPES Buffer (5:1)	[3]

4.	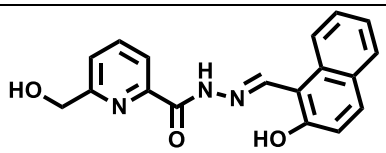	Zn^{2+} (5.7 nM) Cd^{2+} (1.09 µM) Al^{3+} (1.64 µM) F^{-} (21.1 µM) H_2PO4^{-} (2.56 µM)	MeOH/HEPES Buffer (7:3)	[4]
5.	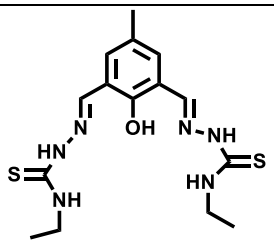	Zn^{2+} (0.59 nM) $H_2PO_4^{-}$ (26 µM)	MeOH/H_2O (4:1)	[5]
6.	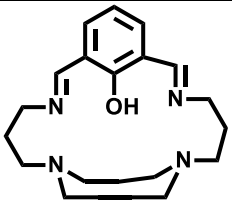	Zn^{2+} (5.4 µM) $H_2PO_4^{-}$ (-)	CH_3CN/HEPES Buffer (1:1)	[6]
7.	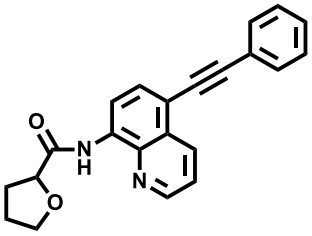	Zn^{2+} (41 nM) $H_2PO_4^{-}$ (49 nM)	DMSO/H_2O (8:2)	[7]
8.	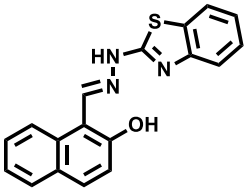	Zn^{2+} (0.65 µM) Cd^{2+} (2.1 µM) $H_2PO_4^{-}$ (-) HPO_4^{2-} (-)	CH_3OH/H_2O (7:3)	[8]
9.	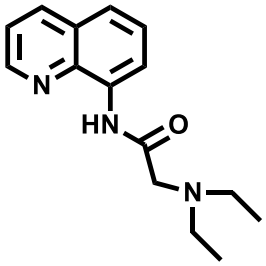	Zn^{2+} (8.8 nM) $H_2PO_4^{-}$ (0.05 µM)	CH_3CN/H_2O (8:2)	[9]

10.	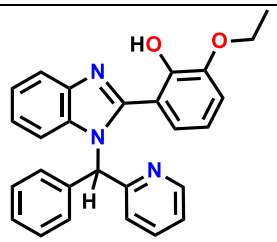	Zn^{2+} (3.2 nM) $H_2PO_4^-$ (0.238 µM)	9:1 (v/v) DMSO/H_2O	This Work

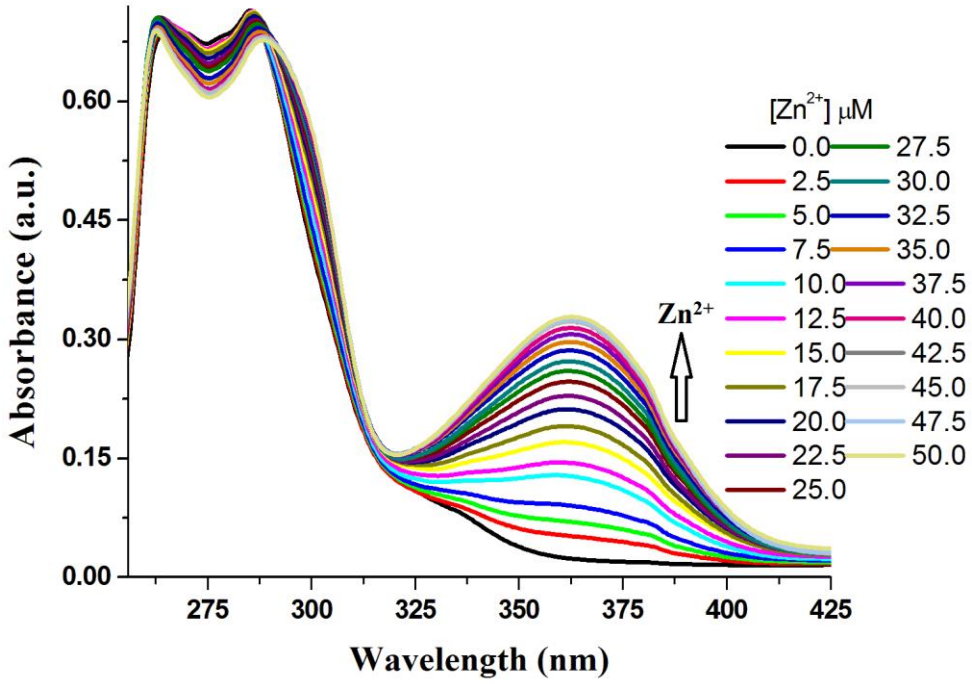

Fig. S9 Change in the absorption spectrum of HL (50 µM) on gradual addition of Zn^{2+} ion (0-50 µM).

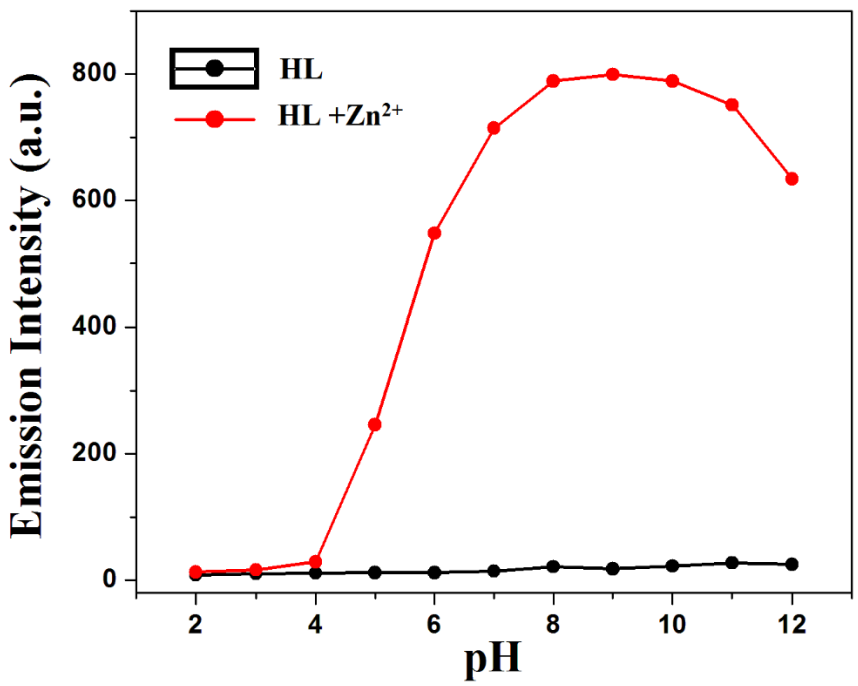

Fig. S10 pH effect on HL for Zn^{2+} sensing.

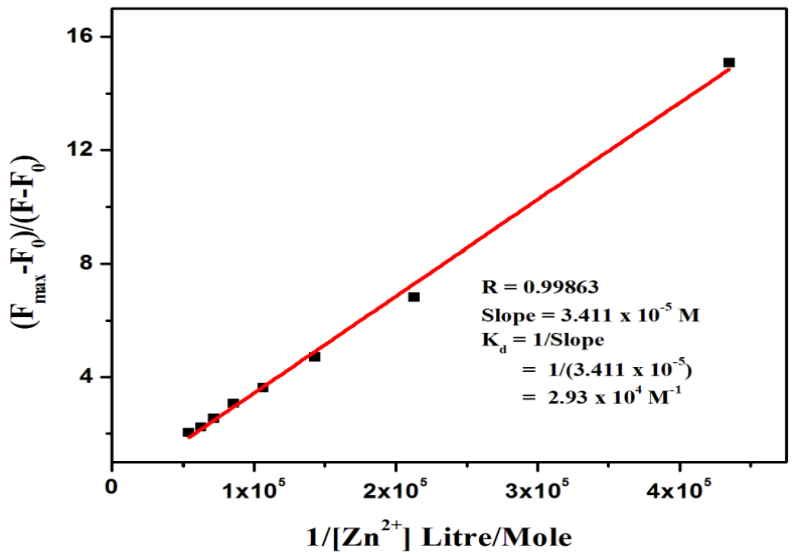

Fig. S11 Binding constant K_d evaluated from Benesi-Hildebrand plot of probe HL towards Zn^{2+} ion.

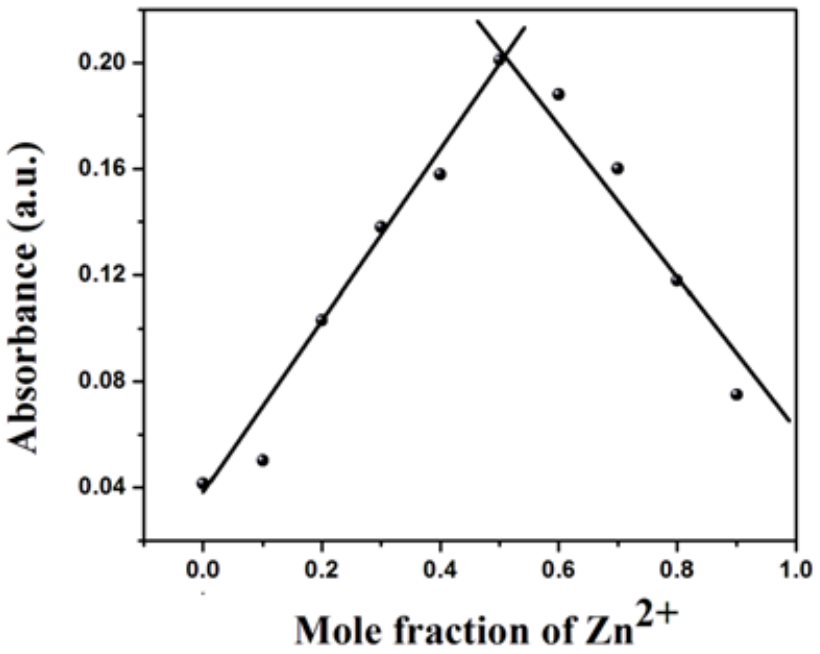

Fig. S12 Job's plot between $Zn^{2+}$and HL.

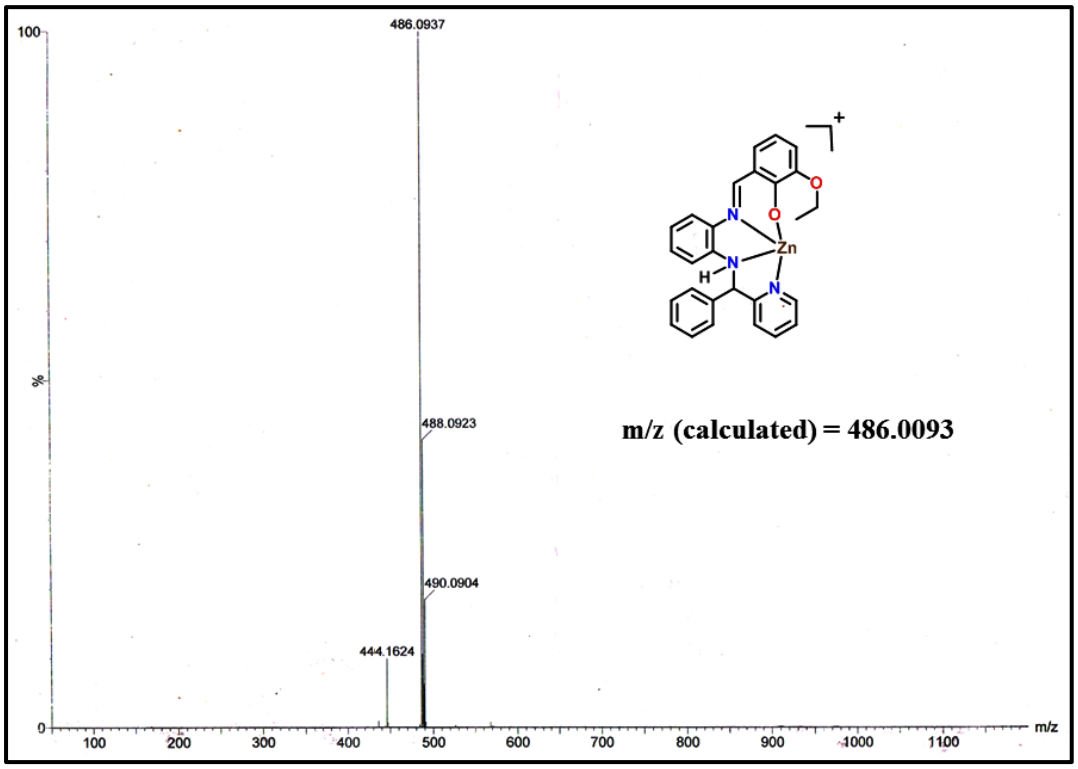

Fig. S13 ESI-MS spectrum of HL-Zn^{2+} complex.

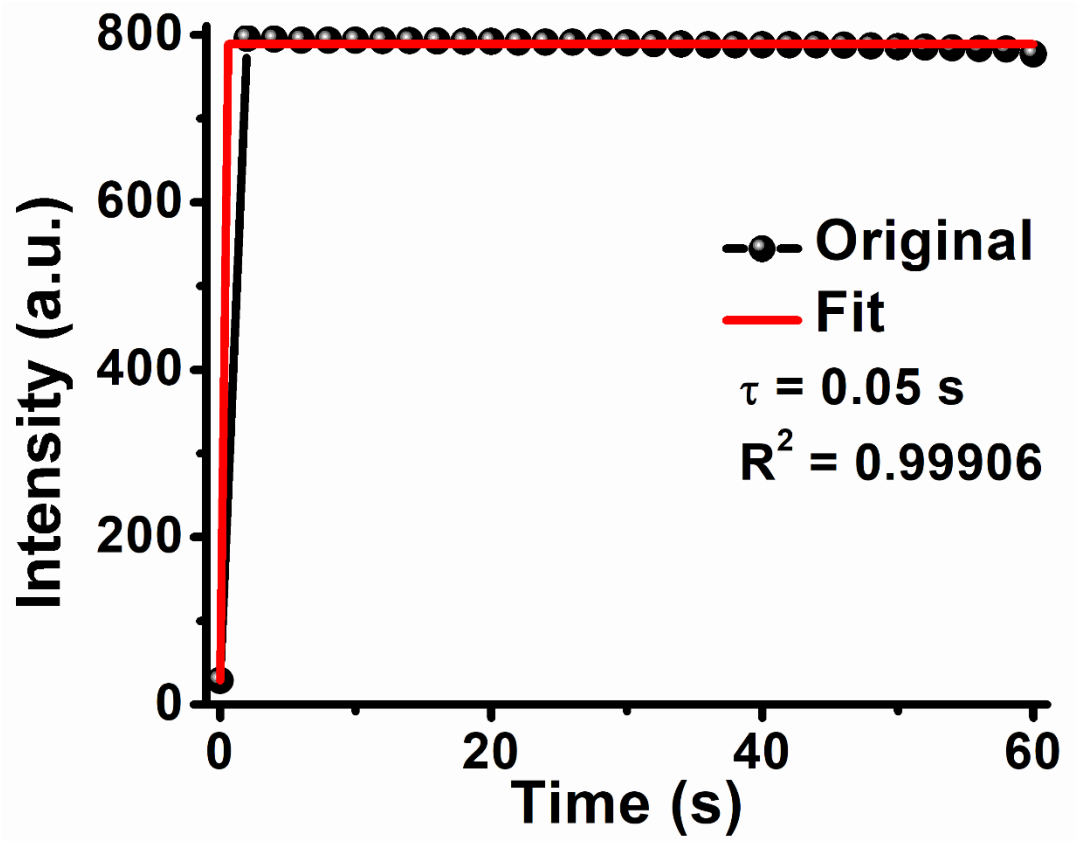

Fig. S14 Time-course of emission intensity of HL upon addition of 1 equivalent Zn^{2}.

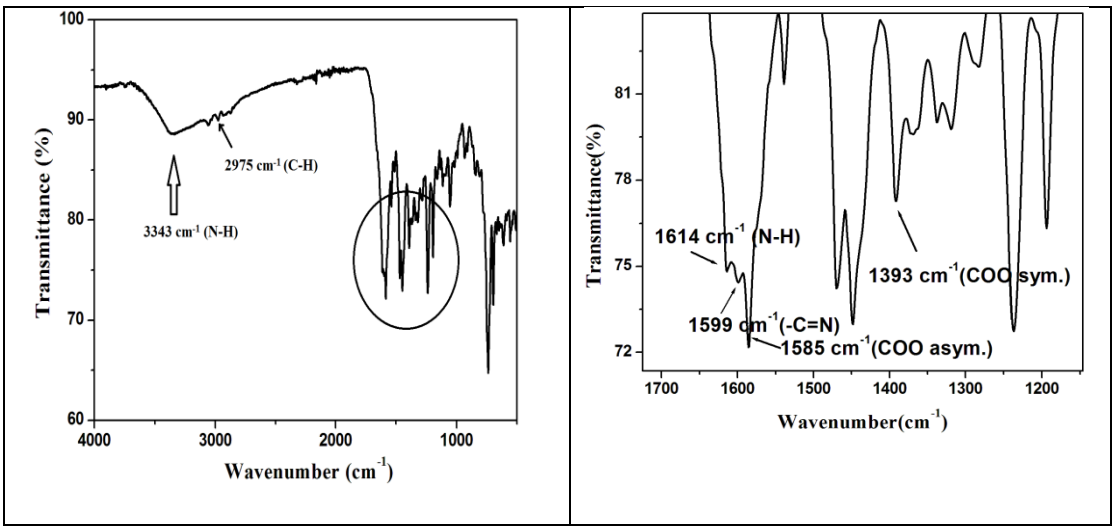

Fig. S15 IR spectrum of HL-Zn^{2+} complex; Right: zoom image in wavenumber around 1200-1700 cm^{-1}.

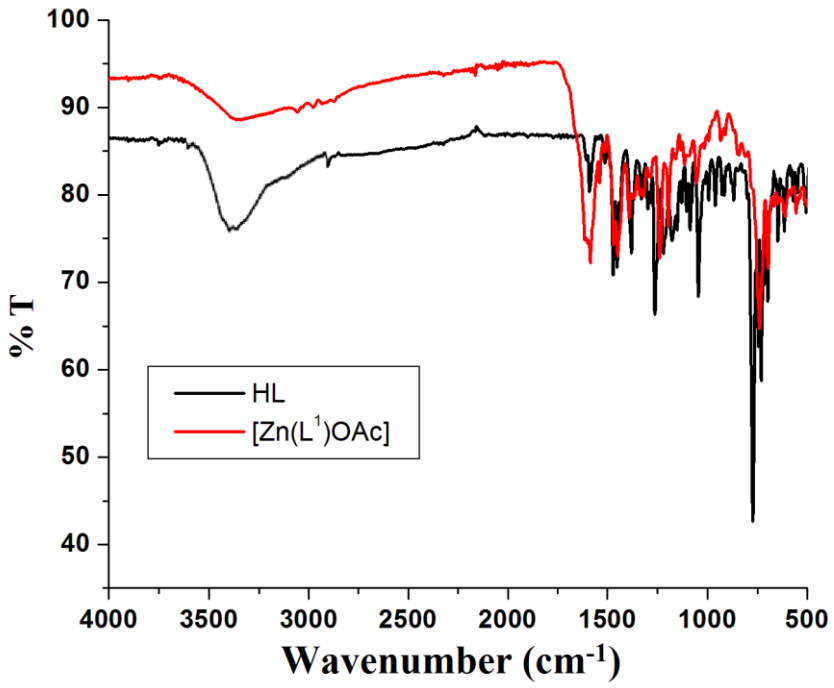

Fig. S16 Merge IR spectrum of HL and HL-Zn^{2+} complex ([Zn(L^1)OAc]).

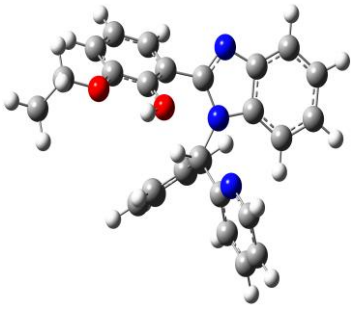	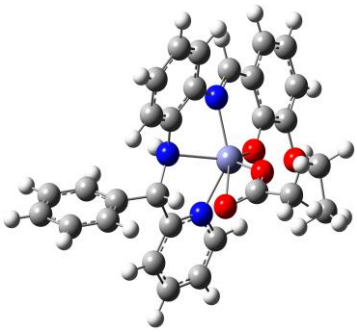
HL	[Zn(L^1)OAc]

Fig. S17 DFT optimized structure of probe HL and its zinc complex using B3LYP method.

Table S4 Some selected bond length of HL obtained from single crystal and compared with theoretical optimized structure.

	Experimental bond length (Å)	**Theoretically calculated bond length (Å)**
C007-N1	1.374(9)	1.39
N1-C7	1.475(10)	1.46
C7-C18	1.527(10)	1.53
C18-N3	1.392(12)	1.33
C7-H7	0.98	1.08
C007-N2	1.307(9)	1.31
C007-C5	1.497(10)	1.47
C5-C6	1.390(10)	1.39
C6-O2	1.366(9)	1.36
O2-H2	0.82	0.96
C1-C6	1.392(10)	1.40
C1-O1	1.383(9)	1.37

Table S5 Selected bond angles of probe HL from the crystal unit and its comparison with the optimized structure.

Bond Angles	**Experimental angle(°)**	**Theoretically calculated Angle(°)**
C007-N1-C7	124.5(5)	124.89
N1-C7-C18	112.1(6)	111.70
C7-C18-N3	118.7(7)	115.06
C18-N3-C14	118.4(8)	118.48
N1-C007-N2	112.6(6)	113.01
C007-N2-C9	105.2(6)	105.60

N2-C007-C5	123.4(6)	121.69
C007-C5-C6	120.9(6)	123.14
C6-C5-O2	118.0(6)	120.16
C6-C1-O1	114.5(7)	113.28
C6-O2-H2	110	107.78

Table S6 Selected frontier molecular orbitals of HL along with their energies.

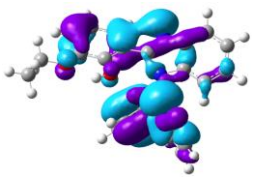	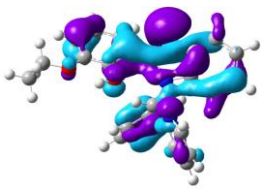	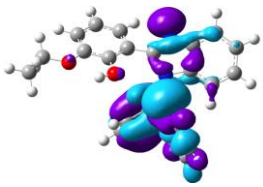	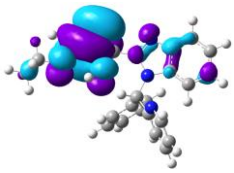
HOMO-5	HOMO-4	HOMO-3	HOMO-2
-7.150 eV	-6.957 eV	-6.888 eV	-6.047 eV
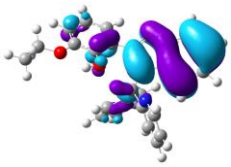	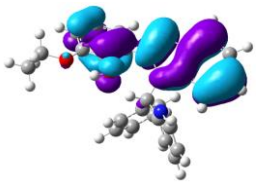	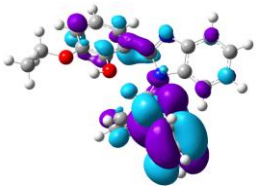	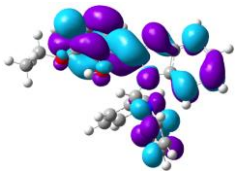
HOMO-1	HOMO	LUMO	LUMO+1
-5.980 eV	-5.826 eV	-1.280 eV	-0.919 eV
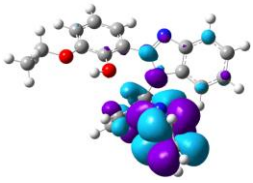	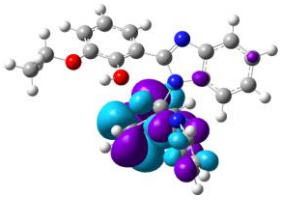	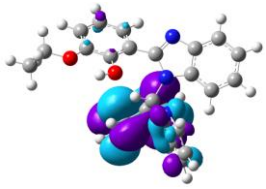	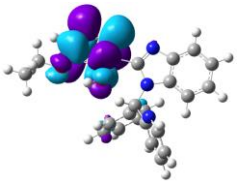
LUMO+2	LUMO+3	LUMO+4	LUMO+5
-0.821 eV	-0.630 eV	0.518 eV	0.442 eV

Table S7 Selected frontier molecular orbitals of [Zn(L^1)OAc] complex along with their energies.

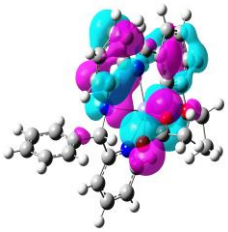	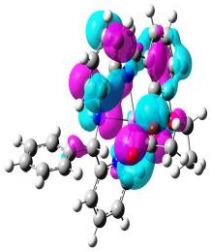	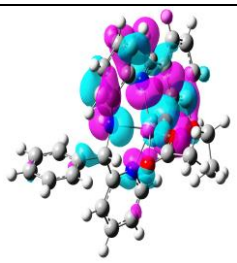	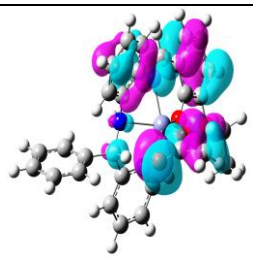
HOMO-5	HOMO-4	HOMO-3	HOMO-2
--6.62 eV	-6.52 eV	-6.42 eV	-5.94 eV
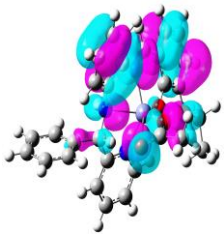	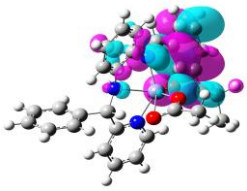	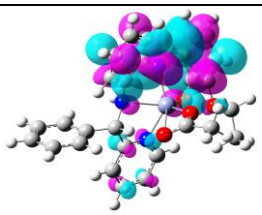	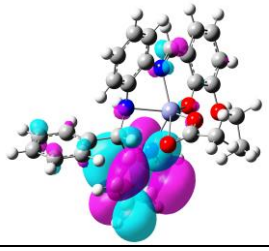
HOMO-1	HOMO	LUMO	LUMO+1
-5.87 eV	-5.0 eV	-1.74 eV	-1.61 eV
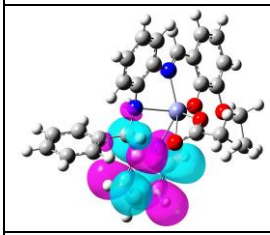	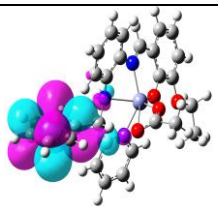	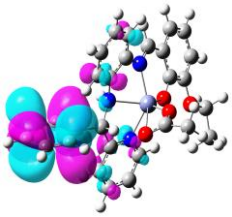	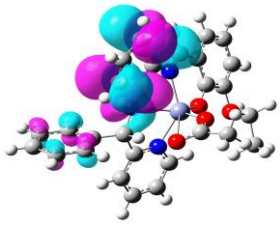
LUMO+2	LUMO+3	LUMO+4	LUMO+5
-1.03 eV	-0.69 eV	-0.58 eV	-0.3 eV

Table S8 Probable electronic transition of HL from TD-DFT calculation.

Excitation Energy (eV)	Wavelength Exp. (nm)	Wavelength Theor. (nm)	Oscillator strength	Key Transition	Nature of Transition
4.2538	335	291.47	0.0589	HOMO-1→ LUMO	ILCT
4.3614	285	284.28	0.0937	HOMO-2→ LUMO	ILCT
4.6384	265	267.30	0.0935	HOMO-2→ LUMO+1	ILCT

Table S9 Probable electronic transition of [Zn(L^1)OAc] from TD-DFT calculation.

Excitation Energy	Wavelength Exp. (nm)	Wavelength Theor. (nm)	Oscillation Frequency	Key Transition	Nature of Transition
3.6399 eV	362	340.62	0.4568	HOMO-1 →LUMO	ILCT
4.1028 eV	289	302.19	0.1619	HOMO-2→ LUMO	ILCT

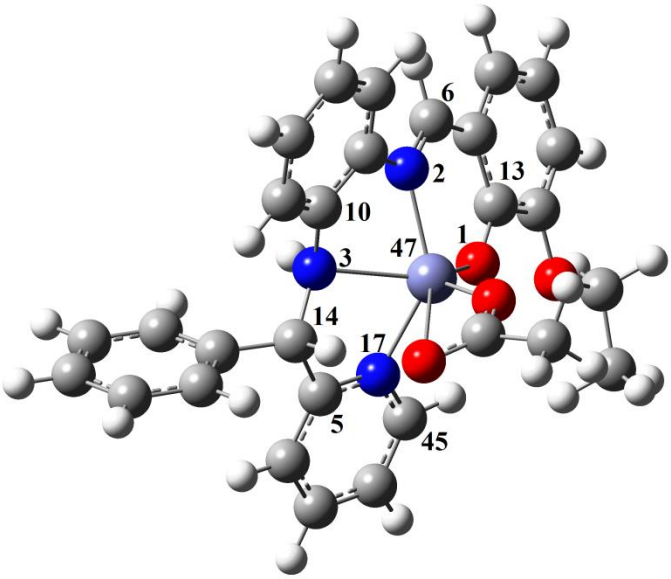

Fig. S18 DFT optimized structure of Zn-complex exhibiting twisting framework.

Table S10 Some selective torsional angles present in the Zn-complex (from DFT-optimized structure).

Bonds	**Angle (°)**
6 – 2 – 47 – 3	-147.25
45 – 17 – 47 – 3	162.40
2 – 47 – 3 – 14	-168.12
17 – 47 – 3 – 10	170.12
13 – 1 – 47 – 17	149.07
1 – 47 – 17 – 5	-158.45

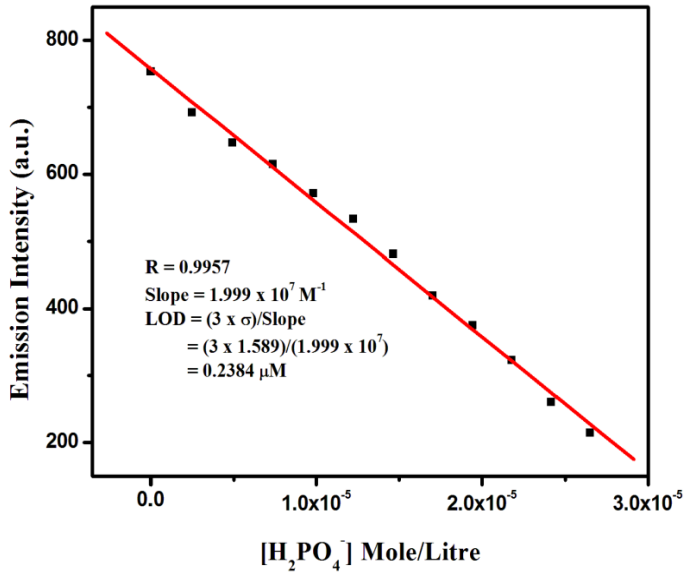

Fig. S19 Limit of detection (LOD) determination for $H_2PO_4^-$ by [Zn(L^1)OAc] complex.

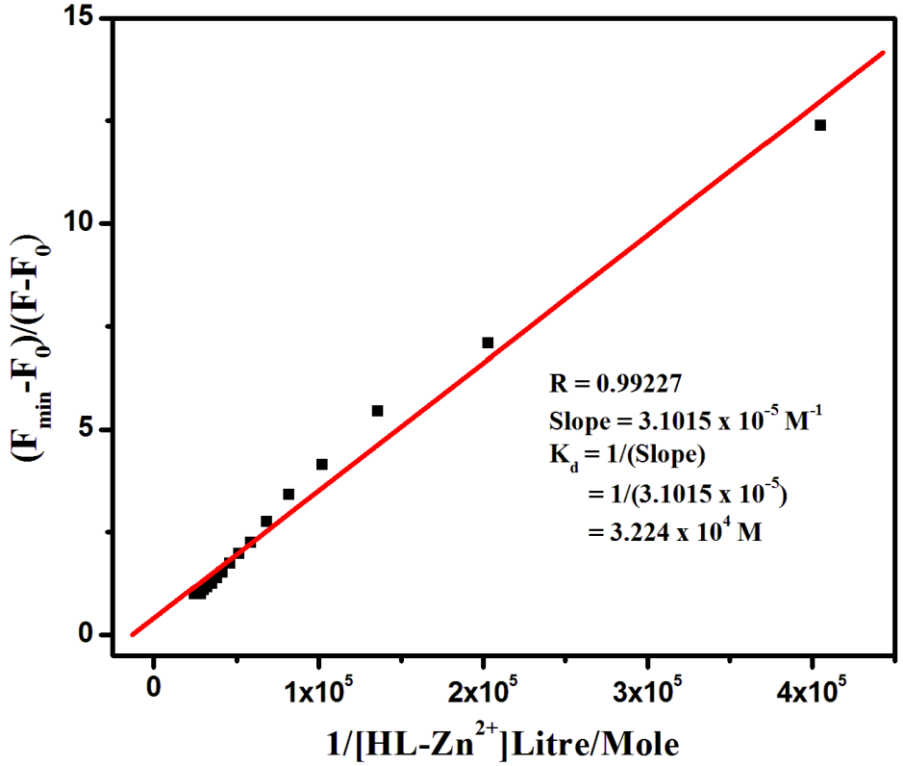

Fig. S20 Binding constant, K_d for $H_2PO_4^-$.

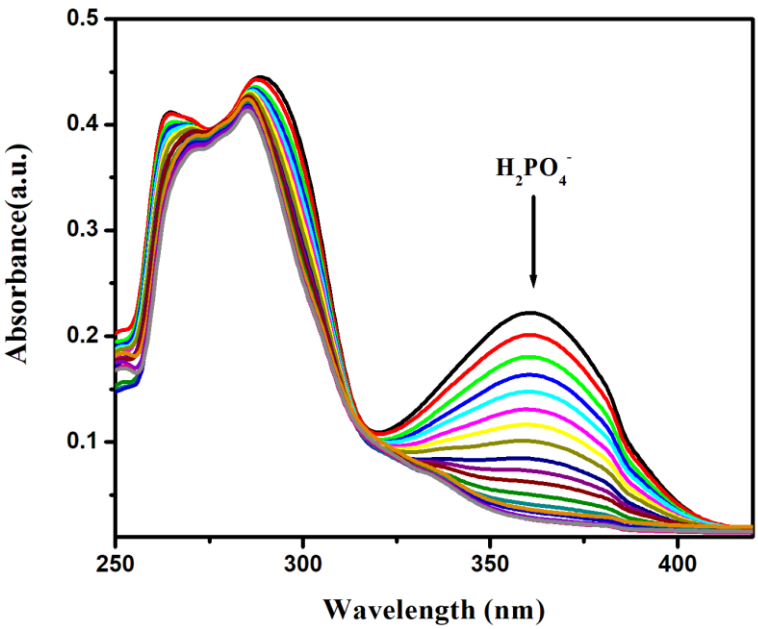

Fig. S21 Change in UV-Vis absorption spectra of [Zn(L^1)OAc] on gradual addition of $H_2PO_4^-$.

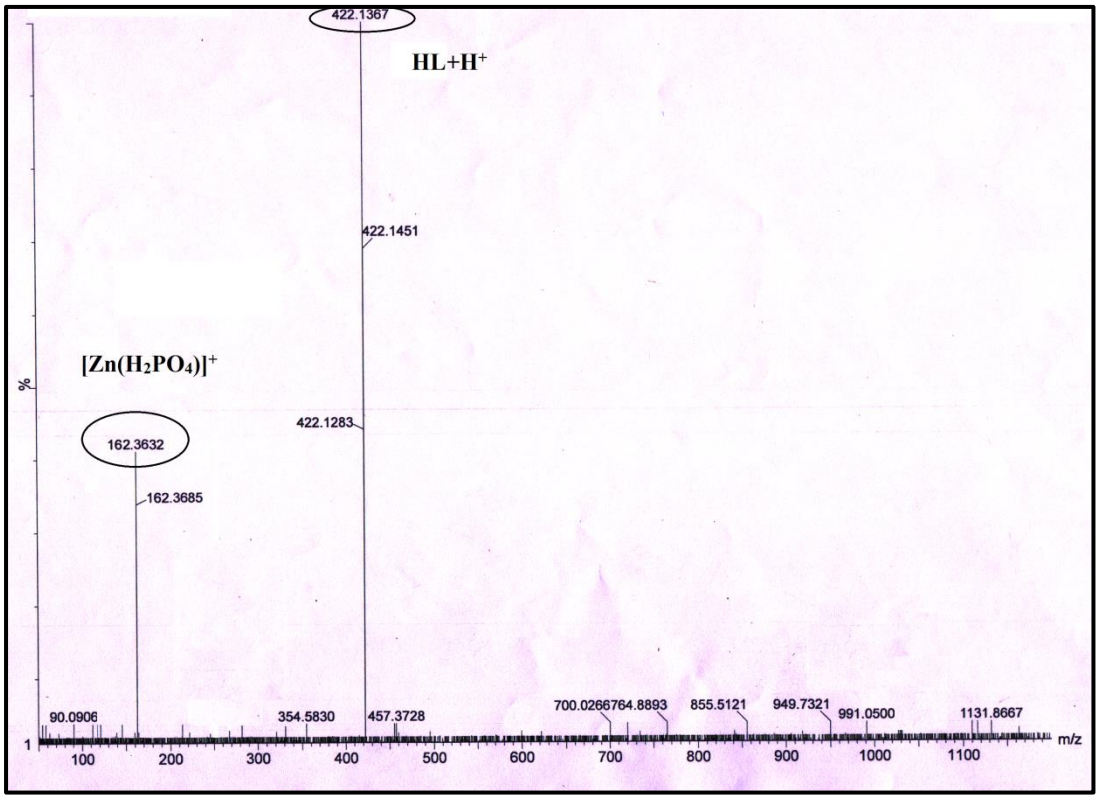

Fig. S22 ESI-MS spectrum in addition of $H_2PO_4^-$ to the in-situ generated HL -Zn^{2+} complex.

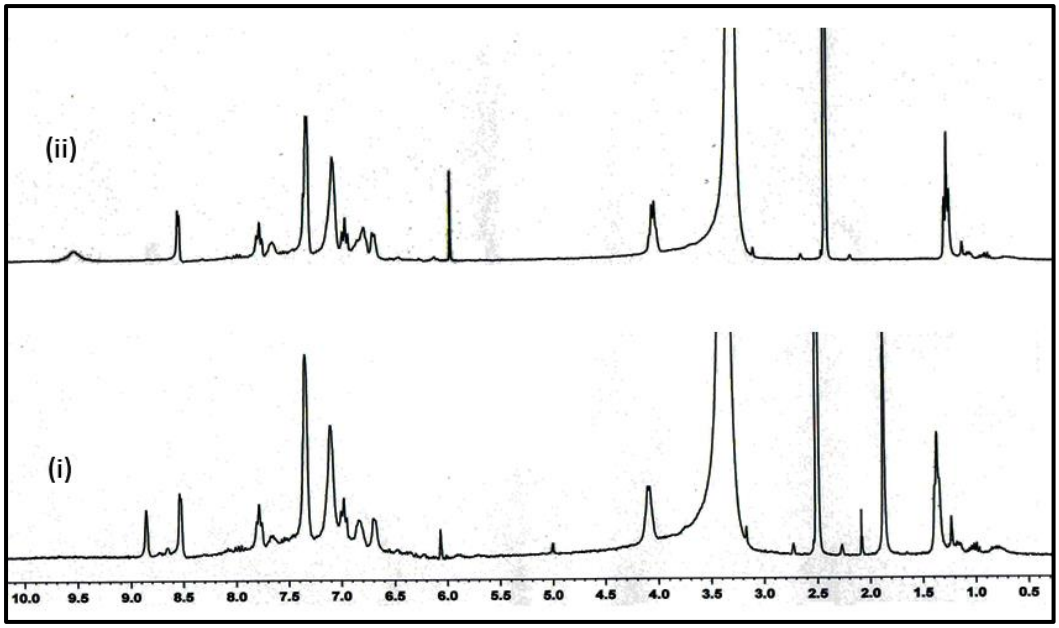

Fig. S23 ^{1}H NMR spectra (i) HL+Zn^{2+} (1.0 eqv.) and (ii) HL+Zn^{2+} (1.0 eqv.)+ $H_2PO_4^-$ (1.0 eqv.).

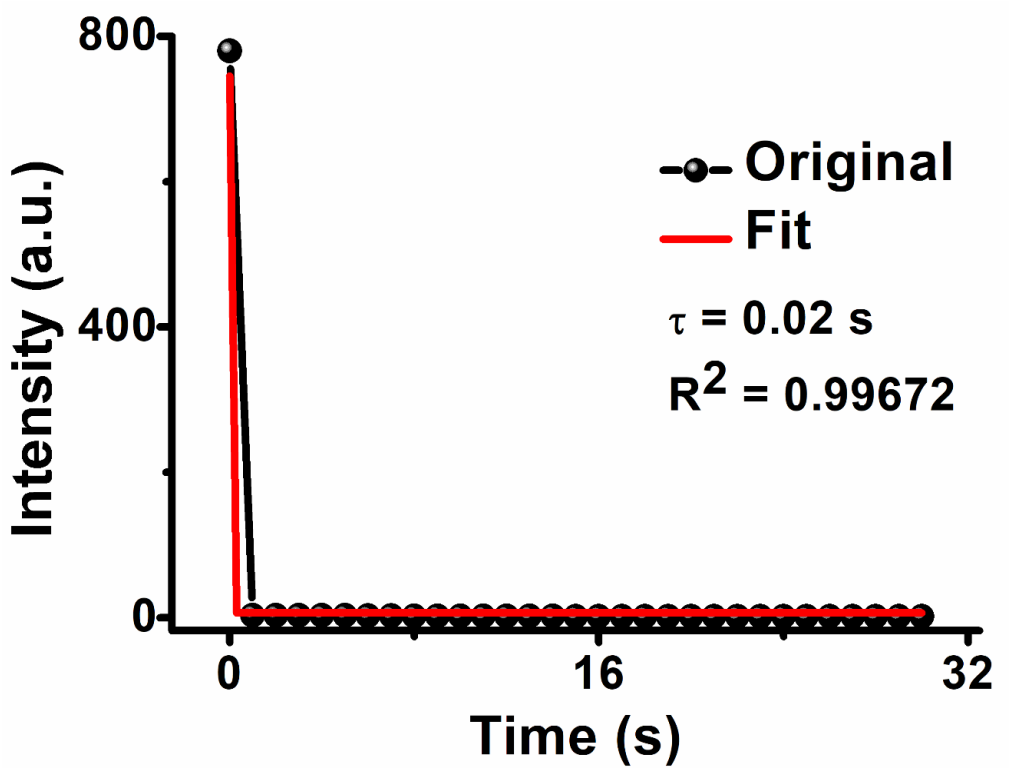

Fig. S24 Time-course of intensity quenching of [Zn(L^1)OAc] upon addition of 1 equivalent $H_2PO_4^-$.

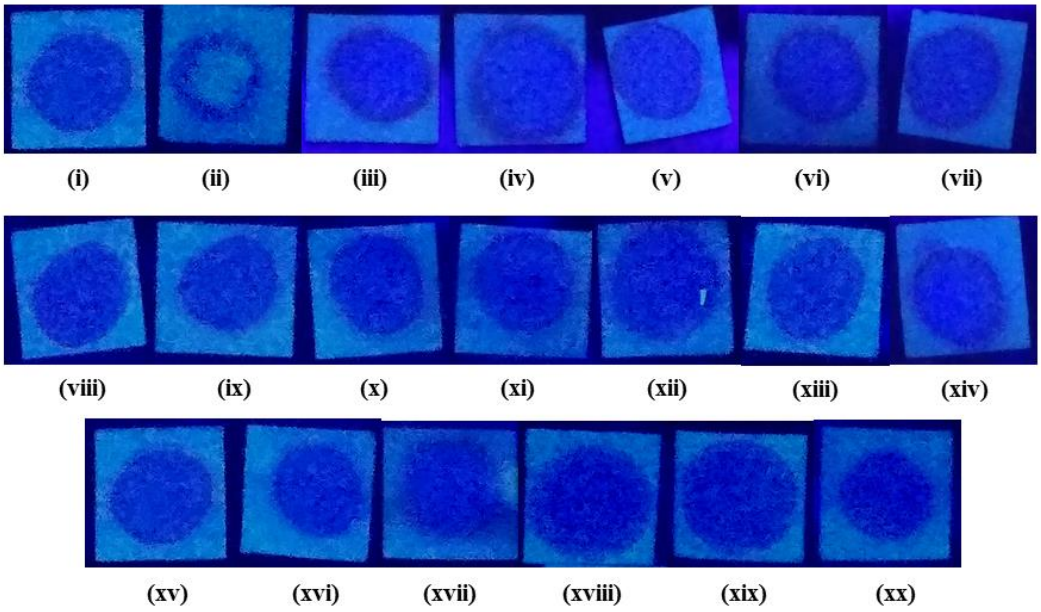

Fig. S25 Paper kit detection: Zn-complex in presence of different anions; (i) [Zn(L^1)OAc], (ii) $H_2PO_4^-$, (iii) I^-, (iv) Br^-, (v) Cl^-, (vi) $H_2PO_4^-$, (vii) S^{2-}, (viii) PO_4^{3-}, (ix) $S_2O_3^{2-}$, (xx) IO_3^-, (xi) citrate, (xii) AcO^-, (xiii) F^-, (xiv) AsO_2^-, (xv) AsO_3^{3-}, (xvi) CN^-, (xvii) SCN^-, (xviii) SO_4^{2-}, (xix) NO_2^-, (xx) NO_3^-.

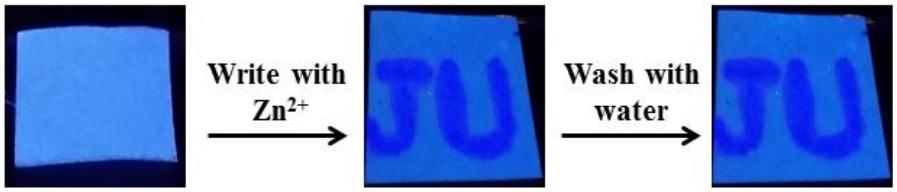

Fig. S26 Photographs of **HL** coated filter paper with hand written images and after washing with water; λ_{ex}, 365 nm.

References

1 Y. Liu, X. Wang, E. Feng, C. Fan and S. Pu, *Spectrochim. Acta A*, 2021, **246**, 119052.

2 M. An, B. Kim, H. Seo, A. Helal and H. Kim, *Spectrochim. Acta A*, 2016, **169**, 87–94.

3 J. Fu, K. Yao, B. Li, H. Mei, Y. Chang and K. Xu, *Spectrochim. Acta A*, 2020, **228**, 117790.

4 N. Behera and V. Manivannan, *J. Photoch. Photobio. A*, 2018, **353**, 77–85.

5 R. Purkait, A. D. Mahapatra, D. Chattopadhyay and C. Sinha, *Spectrochim. Acta A*, 2019, **207**, 164–172.

6 S. Goswami, S. Maity, A. C Maity, A. K. Das, K. Khanra, T. K. Mandal and N. Bhattacharyya, *Tetrahedron Lett.*, 2014, **55**, 5993–5997.

7 K. Du, S. Niu, L. Qiao, Y. Dou, Q. Zhu, X. Chen and P. Zhang, *RSC Adv.*, 2017, **7**, 40615–40620.

8 A. Gogoi, S. Samanta and G. Das, *Sens. Actuators B*, 2014, **202**, 788–794.

9 S. S. Kumara, R. S. Kumara and S. K. A. Kumara, *Inorg. Chim. Acta*, 2020, **502**, 119348.